Acta Pharmaceutica Sinica B 2024;14(6):2581−2597

Chinese Pharmaceutical Association
Institute of Materia Medica, Chinese Academy of Medical Sciences

Acta Pharmaceutica Sinica B

www.elsevier.com/locate/apsb
www.sciencedirect.com

ORIGINAL ARTICLE

Idebenone alleviates doxorubicin-induced cardiotoxicity by stabilizing FSP1 to inhibit ferroptosis

Hongliang Qiu[a,b,†], Sihui Huang[a,b,†], Yuting Liu[a,b,†], Libo Liu[a,b], Fengming Guo[a,b], Yingying Guo[a,b], Dan Li[a,b], Xianfeng Cen[a,b], Yajie Chen[a,b], Meng Zhang[a,b], Yan Che[a,b], Man Xu[a,b,*], Qizhu Tang[a,b,*]

[a]*Department of Cardiology, Renmin Hospital of Wuhan University, Wuhan 430060, China*
[b]*Hubei Key Laboratory of Metabolic and Chronic Diseases, Wuhan 430060, China*

Received 18 October 2023; received in revised form 8 January 2024; accepted 4 February 2024

KEY WORDS

Idebenone;
DOX-induced cardiotoxicity;
Ferroptosis;
FSP1;
Ubiquitination;
Lipid peroxidation;
Iron overload;
Clinical translation

Abstract Doxorubicin (DOX)-mediated cardiotoxicity can exacerbate mortality in oncology patients, but related pharmacotherapeutic measures are relatively limited. Ferroptosis was recently identified as a major mechanism of DOX-induced cardiotoxicity. Idebenone, a novel ferroptosis inhibitor, is a well-described clinical drug widely used. However, its role and pathological mechanism in DOX-induced cardiotoxicity are still unclear. In this study, we demonstrated the effects of idebenone on DOX-induced cardiotoxicity and elucidated its underlying mechanism. A single intraperitoneal injection of DOX (15 mg/kg) was administrated to establish DOX-induced cardiotoxicity. The results showed that idebenone significantly attenuated DOX-induced cardiac dysfunction due to its ability to regulate acute DOX-induced Fe^{2+} and ROS overload, which resulted in ferroptosis. CESTA and BLI further revealed that idebenone's anti-ferroptosis effect was mediated by FSP1. Interestingly, idebenone increased FSP1 protein levels but did not affect *Fsp1* mRNA levels in the presence of DOX. Idebenone could form stable hydrogen bonds with FSP1 protein at K355, which may influence its association with ubiquitin. The results confirmed that idebenone stabilized FSP1 protein levels by inhibiting its ubiquitination degradation. In conclusion, this study demonstrates idebenone attenuated DOX-induced cardiotoxicity by inhibiting ferroptosis *via* regulation of FSP1, making it a potential clinical drug for patients receiving DOX treatment.

*Corresponding authors.
E-mail addresses: qztang@whu.edu.cn (Qizhu Tang), xuman987@whu.edu.cn (Man Xu).
[†]These authors made equal contributions to this work.
Peer review under the responsibility of Chinese Pharmaceutical Association and Institute of Materia Medica, Chinese Academy of Medical Sciences.

https://doi.org/10.1016/j.apsb.2024.03.015

1. Introduction

Doxorubicin (DOX) is a classical anthracycline chemotherapy drug widely used in clinics. However, due to its nonspecific cytotoxic properties, DOX is limited in clinical use to the extent that it is likely to induce cardiac injuries called DOX-induced cardiotoxicity. Three Phase III studies have indicated that 26% of patients would experience DOX-related congestive heart failure compared with placebo-treated patients[1]. Although the mechanisms of DOX-induced cardiotoxicity are complicated, it is universally accepted that cell death like apoptosis, autophagy, and pyroptosis account for most. And excessive ROS activation and disturbance of iron metabolism play a crucial role in DOX-induced cardiotoxicity[2,3]. Recently, researchers have indicated that ferroptosis, a novel cell death program, is also a crucial mechanism of DOX-induced cardiotoxicity, and targeting ferroptosis is beneficial for treating DOX-induced cardiotoxicity[4−6].

Ferroptosis, a novel form of regulated cell death, is characterized by iron-dependent excessive lipid peroxidation[7]. Essentially, ferroptosis is determined by metabolism factors including iron, ROS, and membrane lipids. Excessive Fe^{2+} in cells generates ROS through the Fenton reaction, and lipids in mitochondrial or cell membranes are peroxidized. Several studies demonstrated that there are multiple antioxidant mechanisms to regulate iron metabolism and eliminate excess toxic ROS, including GPX4/GSH[8,9], FSP1/CoQ_{10}[10], and DHODH/CoQ_{10}[11] axis. As a classic anti-ferroptosis target, GPX4 has been extensively investigated. While FSP1, as a novel anti-ferroptosis target independent of GPX4, its specific mechanism is still unclear in DOX-induced cardiotoxicity. Mechanically, FSP1 (formerly AIFM2) is a CoQ_{10} oxidoreductase, which protects against ferroptosis by producing ubiquinol to trap lipid radicals[10]. Recent studies have shown that targeting GPX4 systems can effectively resist DOX-induced cardiotoxicity[4], but the role of FSP1 is still unclear.

Idebenone (Supporting Information Fig. S1A), a CoQ_{10} analogue, is a common clinical drug used to improve brain metabolism and mental symptoms since it is safe and well-tolerated in clinical trials[12]. Compared to CoQ_{10}, idebenone contains the same redox-active benzoquinone moiety, but with a significantly shorter lipophilic side chain and a terminal hydroxyl group to increase its solubility[13]. CoQ_{10} has been widely used in cardiovascular diseases, but research related to idebenone is rare. A previous study has demonstrated that idebenone protects against atherosclerosis by inhibiting the activation of NLPR3[14]. Additionally, idebenone has a strong antioxidant effect, and it could prevent lipid peroxidation and remove oxygen-derived free radicals, implying its role in ferroptosis.

In this study, we investigated the mechanism of idebenone by constructing a DOX-induced cardiotoxicity model *in vitro* and *in vivo*. We demonstrated that idebenone attenuates DOX-induced cardiotoxicity by inhibiting ferroptosis. Idebenone up-regulates FSP1 protein levels to enhance the reduction of CoQ_{10} to $CoQ_{10}H_2$, effectively eliminating excessive ROS and regulating iron homeostasis. More importantly, idebenone stably binds to FSP1 through hydrogen bonds, inhibiting FSP1 ubiquitin−proteasome degradation.

2. Materials and methods

2.1. Animals and treatments

The animal care and experimental methods complied with the Guidelines for the Care and Use of Laboratory Animals published by the National Institutes of Health (NIH Publication, revised 2011) and approved by the Animal Care and Use Committee of Renmin Hospital of Wuhan University (Approval Number: WDRM-20210505). C57BL/6J male mice (8 weeks old, 23−25 g) were purchased from the Institute of Laboratory Animal Science, Chinese Academy of Medical Sciences (Beijing, China) and fed adaptively for 1 week before experimentation. All mice were maintained under specific pathogen-free, environmentally controlled (Temperature: 20−25 °C; Humidity: 50 ± 5%) barrier conditions in individually ventilated cages and given free access to water and food.

The animals were randomly assigned into four groups (n = 12 per group): saline-treated group (Ctrl), idebenone-treated group (IDBN), DOX-treated group (DOX), and DOX and idebenone-treated group (DOX + IDBN). To generate DOX-induced cardiotoxicity, the mice were given a single intraperitoneal injection of DOX (15 mg/kg dissolved in sterile saline, MCE, HY-15142), and the control group were given an equal amount of normal saline referring to our previous study[15]. Mice divided into the IDBN or DOX + IDBN group were treated with idebenone (200 mg/kg/day dissolved in sterile saline, MCE, HY-N0303) by oral gavage for 7 days before and after DOX treatment. Seven days after the injection of DOX, echocardiography was implemented.

To specifically overexpress FSP1 in the mouse heart, we constructed an adeno-associated virus serotype 9 (AAV9) viral vector carrying FSP1 (AAV9-FSP1) (Supporting Information Fig. S7A−S7C), and used AAV9-NC as a negative control (OBiO, Shanghai). After 4 weeks of tail intravenous injection of AAV9-FSP1 or AAV9-NC (1×10^{12} vg per mouse), the mice were divided into four groups: AAV9-NC, AAV9-FSP1, AAV9-NC + DOX, and AAV9-FSP1+DOX. Then, the mice were given a single intraperitoneal injection of DOX (15 mg/kg dissolved in sterile saline, MCE), and the control group was given normal saline. The subsequent experiments were conducted after 7 days of DOX administration.

2.2. Echocardiography

For measuring mice's cardiac function, mice were given 1.5% isoflurane anaesthesia and then put on a heating pad. Transthoracic echocardiography was analyzed with a 10-MHz linear array ultrasound transducer equipped with a 30-MHz probe (Vevo 3100 system Visual Sonics) as described in our previous study[16,17]. The echocardiographic parameters, including left ventricular ejection fraction (LVEF), left ventricular fractional shortening (LVFS) and left ventricular end-systolic dimension (LVESd) were calculated and averaged from at least five consecutive cardiac cycles.

2.3. Histological staining

The hearts were fixed in 10% formalin, treated with dehydration and embedding, and then serially sectioned at 5 μm thickness. According to the manufacturer's instructions, heart sections were stained with haematoxylin and eosin (H&E) to examine cardiac histological morphology. To assess myocardial fibrosis, cardiac sections were stained with picro-sirius red (PSR) and Masson's trichrome. TUNEL staining was used to detect apoptosis according to the manufacturer's instructions (Beyotime, Shanghai). The images were then captured by a fluorescence microscope (Olympus DX51, Japan) and analyzed with Image-Pro Plus version 6.0 (MD, USA).

2.4. Cell culture and treatment

Neonatal rat cardiomyocytes (NRCMs) were isolated from 1- to 2-day-old neonatal Sprague−Dawley rats as previously described[16]. Briefly, the hearts of rats were removed and cut into pieces measuring 1−3 mm^3. Then the heart tissues were digested with 0.125% trypsin−EDTA (2520-072; Gibco, USA) for 15 min × 5 times, subsequently collected and stopped in Dulbecco's modified Eagle's medium/F-12 (C11330500BT, Gibco, USA) containing 20% fetal bovine serum (FBS, 10,099-141, Gibco, USA). The digested cells were filtered after centrifugation and incubated for 90 min to remove noncardiac myocytes. After 24 h of culture, cardiomyocytes were plated and cultured in fresh DMEM/F12 containing 10% FBS.

The cells were randomly divided into the following four treatment groups: (a) control group (Ctrl), (b) 5 μmol/L idebenone group (IDBN), (c) 1 μmol/L DOX group (DOX), (d) 1 μmol/L DOX + 5 μmol/L idebenone group (DOX + IDBN). For better storage, DOX was dissolved in DMSO to 1 mmnol/L and idebenone was dissolved in PBS to 20 mmol/L. After 24 h of cell incubation with different treatments, cells were collected for mRNA or protein analysis. Each experiment in this study was repeated at least three times, with one sample representing one independent replication.

2.5. Cell viability examining

According to the manufacturer's instructions, we determined the viability of NRCMs using the cell counting kit-8 assay (CCK-8, Beyotime, Shanghai, China). Before the following experiments, NRCMs were seeded in 96-well plates at a density of 4×10^4 cells/well for 48 h. To test idebenone's cytotoxicity, the cells were treated with different concentrations of idebenone (0, 0.1, 0.2,0.5, 1, 2, 5, 10, or 50 μmol/L) with or without DOX (1 μmol/L). After incubating for 24 h, the cell viability was examined by CCK-8. Then, we analyzed the absorbance at 450 nm using a microplate reader (Synergy HT; Agilent Technologies, Inc.). A concentration of 5 μmol/L was chosen for further cellular experiments.

2.6. si-RNA transfection

First, we measured the inhibitory efficiency of si-FSP1 at different concentrations. The NRCMs were seeded in six-well plates and cultured for 48 h. Then, si-FSP1 (with sense strand 5′-CGGUGACCUUCAAGGACAATT-3′, antisense 5′-UUGUCCUUGAAGGUCACCGTT-3′) was transfected into NRCMs using Lipofectamine® 6000 transfection reagent at concentrations of 20, 50 or 100 nmol/L, according to the manufacturer's instructions. Following transfection for 48 h, mRNA levels were evaluated to determine inhibition efficiency and 50 nmol/L was selected for subsequent experiments.

After si-FSP1 transfection, we then replaced the medium with a fresh medium and treated the cells with DOX (1 μmol/L) in the presence or absence of idebenone (5 μmol/L) for another 24 h. Next, to detect the expression of related genes and proteins, NRCMs were harvested and subjected to RT-PCR and Western blotting.

2.7. Plasmids construction and transfection

Recombinant full-length and mutant plasmids pCMV-FSP1-WT-HA, pCMV-FSP1-K118R-HA and pCMV-FSP1-K355R-HA were purchased from Miaoling Biology. The FSP1 mutant plasmids were obtained by mutating the lysine at the K118 and K355 positions of the FSP1 full-length sequence to arginine. Following plasmid construction, the plasmids were transfected into HEK 293T cells. In brief, HEK 293T cells were cultured to 70% density, and the plasmid was transfected into the cells with the transfection reagent Lipofectamine 6000 (Beyotime, Shanghai) for 24 h. After transfection, cells were collected for further experiments such as Co-IP.

2.8. Oxidative stress assays

ROS levels were evaluated by DCFH-DA staining *in vitro* and dihydroethidium (DHE) staining *in vivo*. Briefly, NRCMs were incubated with DCFH-DA (5 μmol/L) at 37 °C for 30 min, then washed three times with PBS. Then, ROS levels in NRCMs were assessed using a fluorescence microscope and Beckman Flow cytometry (Beckman Coulter CytoFlex, USA). The heart paraffin sections were incubated with DHE (5 μmol/L) at 37 °C for 30 min, washed three times with PBS, and then counterstained nucleus with DAPI. Lipid peroxidation was measured using C11-BODIPY 581/591 *in vitro*. Briefly, the cells were incubated in 2 μmol/L C11-BODIPY581/591 at 37 °C for 30 min in the dark. The images were captured under an Olympus DX51 fluorescence microscope (Tokyo, Japan) and the fluorescence intensity was measured using Image-J. Tissue and cell MDA were measured using the thiobarbituric acid reactive substances (TBARS) assay kit (Beyotime, Shanghai, China). Specifically, MDA was reacted with thiobarbituric acid at 100 °C, and the MDA-TBA adduct was measured by fluorometry at 532 nm using a microplate reader (Synergy HT; Agilent Technologies, Inc.). To further assess oxidative stress levels, we measured the cardiac total SOD activity, GSH and GSH-Px activity according to the manufacturer's instructions (Beyotime, Shanghai, China).

2.9. Prussian blue staining

Cardiac iron level was measured by Prussian blue stain kit (Abcam, ab150674). According to the manufacturer's instructions, sections of cardiac tissue were incubated within xylene for dewaxing and then gradient ethanol solution for hydration. For the iron stain solution, potassium ferrocyanide solution and hydrochloric acid solution were mixed equally.

2.10. JC-1 staining

JC-1 fluorescent probe (Beyotime, Shanghai) was used to measure mitochondrial membrane potential in NRCMs. NRCMs were treated with DOX for 24 h with or without idebenone, then incubated with JC-1 working solution for 30 min at 37 °C. The cells were then washed at least three times with JC-1 buffer solution. The images were observed under an Olympus DX51 fluorescence microscope (Tokyo, Japan). And the degree of mitochondrial damage was derived from the ratio of red/green fluorescence intensity.

2.11. Transmission electron microscope

Fresh mouse left ventricular heart tissue samples (1 mm^3) were isolated and fixed with 3% glutaraldehyde phosphate. The Microscopy Center of Renmin Hospital of Wuhan University performed post-fixation, embedding, cutting and mounting of the samples. Cardiomyocyte mitochondria were observed by transmission electron microscopy (TM-3000; Hitachi Ltd., Tokyo, Japan).

2.12. CoQ_{10} and $CoQ_{10}H_2$ measurement

CoQ_{10} and $CoQ_{10}H_2$ were measured by the Elisa kit (Mlbio, shanghai). Briefly, fresh heart tissue or cells are ground in PBS containing protease inhibitors, then sonicated in suspension with an ultrasonic cell disrupter. Afterwards, homogenates are centrifuged at 5000×*g* for 5 min to obtain supernatant. The sample supernatant was added to the microplate and incubated with enzyme conjugate at 37 °C for 60 min. After washed 5 times with 1 × washing solution, substrates A and B were added to each well, and they were incubated at 37 °C for 15 min. Finally, the stop solution was added to each well, and CoQ_{10} and $CoQ_{10}H_2$ levels were measured by fluorometry at 450 nm using a microplate reader.

2.13. Western blot

Ventricular tissues and NRCMs were homogenized in RIPA lysis buffer (Servicebio, Wuhan) including protease and phosphatase inhibitors. The cells or tissues were then sonicated and collected by centrifugation at 12,000 rpm for 30 min at 4 °C (Eppendorf, Germany, 5418R). The isolated protein concentration was quantified by BCA kit (Servicebio, Wuhan), diluted with loading buffer and heated at 95 °C for 5 min. The protein was electrophoresed on SDS-PAGE gels and transferred to PVDF membranes, which were blocked with 5% skimmed milk at room temperature for 1 h and incubated overnight with primary antibodies, followed by the incubation with secondary antibodies at room temperature for 1 h. After that, secondary antibodies were incubated for 1 h at room temperature. Membranes were visualized by the ECL reagent using the Odyssey Infrared Imaging System (LI-COR Biosciences, Lincoln, NE, USA) and analyzed using Image Lab software (v3.0; Bio-Rad Laboratories, Inc.). The antibodies used are listed in Supporting Information Table S1.

2.14. Quantitative real-time PCR

According to the manufacturer's instructions, total RNA was isolated from heart tissues or cells using TRIzol® reagent and reverse transcribed with Maxima First Strand cDNA Synthesis Kit. RT-qPCR was performed with real-time PCR detection system (Roche, 04896866001), using Light Cycler 480 SYBR Green Master Mix. The primers used are listed in Supporting Information Table S2.

2.15. Coimmunoprecipitation

We performed the coimmunoprecipitation test following the manufacturer's instructions (Protein A/G Magnetic Beads, MCE). The isolated NRCMs cells were seeded in a six-well plate and then treated with idebenone (5 μmol/L) or an equivalent amount of vehicle in the presence or absence of DOX (1 μmol/L) for 24 h. Before harvesting, MG-132 was added for 6 h to analyze FSP1 ubiquitin levels. Subsequently, cells were extensively lysed using IP Lysis Buffer containing protease inhibitors. The supernatant was obtained after centrifugation at 12,000 rpm for 15 min, then the supernatant protein was mixed with anti-FSP1 antibody or IgG, and incubated overnight at 4 °C. Afterwards, they were spun at 4 °C for 4 h with Protein A/G Magnetic Beads. The samples were then washed 4 times with Tris-buffer. After adding the SDS-PAGE loading buffer, the sample was boiled at 95 °C for 5 min. FSP1 and ubiquitination protein levels were detected by Western blotting on Input or IP proteins.

2.16. Molecular docking

The Autodock Vina docking program was used for idebenone molecular docking[18]. The molecular structure of the idebenone (CAS No. 58186-27-9) ligand compound was obtained from PubChem. The protein receptor molecules for docking are obtained from the Alphafold or PDB protein database (Supporting Information Fig. S5). After hydroprocessing all receptor and ligand structures, input receptor and ligand PDBQT files were prepared for proteins and ligands using the AutoDock tool. And the size and center coordinates of the corresponding grid box were set according to the protein structure. The Autodock Vina program was runned to pick the binding structure with the highest docking score. PyMol was used to analyze ligand−protein binding modes and interactions.

2.17. Cellular thermal shift assay-Western blot (CETSA-WB)

NRCMs were separated and lysed, and the soluble protein lysate was mixed and aliquoted into PCR tubes. The tubes were incubated with idebenone or PBS for 1 h at room temperature (RT) before the CESTA heat pulse. The solution system was then heated at different temperatures for 3 min, followed by cooling in a thermal cycler at 4 °C for 3 min. After centrifugation for 30 min (12,000 rpm, 4 °C), the soluble protein supernatant was used for Western blotting.

2.18. Biolayer interferometry (BLI)

The binding of idebenone (MCE, HY-N0303, purity 99.36%) to FSP1 (Cayman, recombinant, No. 29611) was measured by BLI using the ForteBio Octet RED96e Analysis System. Briefly, FSP1 protein was dissolved in PBS to make a concentration of 0.4 mg/mL, then biotinylated with Biotinylation Kit G-MM-IGT. Idebenone was diluted with PBS to different concentrations, and equal volumes of PBS served as the control group. The cycle repeats loading baseline time 60 s, association time 120 s, and dissociation time 80 s.

2.19. Molecular dynamic simulation

An all-atom explicit solvent model of the IDBN−FSP1 protein complex was established through GROMACS-2022. The system parameters were selected as follows: the temperature is 310 K, the time is 100 ns, and the water model is TIP3P; the force field used by the protein is AMBER99SB, and the C-terminal and N-terminal are COO− and NH_3+, respectively; the force field of the small molecule is GAFF, which was established using Ambertools. The minimum distance between the complex and the system box is 1 nm. The system box is a cuboid with a box size of 9.68 nm × 6.54 nm × 8.55 nm. All simulations employ periodic boundary conditions. Before running the MD, energy minimization is first performed, and the 50,000-step steepest descent method is used to eliminate spatial conflicts. Next, simulations are performed under the NVT ensemble and the NPT (1 bar) ensemble, both with 0.1 ns to equilibrate the system. In the pressure parameter setting, the Parrinello−Rahman method was used to maintain the pressure at 1 bar; for the temperature parameter, the protein and non-protein groups were coupled to an external heat bath through the velocity scaling coupling method, and the temperature was maintained at 310 K. The Verlet buffer used to update the neighbour list every 10 steps, with a cutoff distance of 1.0 nm. The lengths of all bonds were constrained using the LINCS method (proteins) and the SETTLE algorithm (water molecules), allowing an integration time of 2 fs; a cutoff of 1.0 nm was selected for van der Waals interactions, and the electrostatic interactions were calculated using the particle mesh (PME) method. The actual spatial cutoff value is 1.0 nm. The MM/PBSA method was used to calculate the binding energy between the protein IDBN−FSP1 protein complex. In the MM/PBSA method, the binding free energy (ΔG_binding) between the ligand and the receptor is given by Eq. (1):

$$\Delta G\_\text{binding} = \Delta E_{\text{MM}} + \Delta G_{\text{solv}} - T\Delta S \quad (1)$$

where ΔE_{MM} belongs to the molecular mechanics' term and includes electrostatic interactions (ΔE_{elec}) and van der Waals interaction (ΔE_{vdW}); ΔG_{solv} is a solvation energy term, including polar solvation energy (ΔG_{polar}) and non-polar solvation component ΔG_{surf}. ΔG_{polar} is calculated from the GB model, and ΔG_{suf} is estimated from the solvent-accessible surface area (SASA).

2.20. Statistical analysis

In our study, the results were analyzed using GraphPad Prism 8 and are presented as mean ± standard error of the mean (SEM). The experiments were designed to generate groups of equal size through randomization and blinded analyses, with no data points excluded from analysis. And analyses were performed in a blinded fashion. Tukey's *post hoc* test was used to analyze comparisons between multiple groups, while Student's *t*-test was used to evaluate comparisons between two groups. $P < 0.05$ was considered statistically significant.

3. Results

3.1. Idebenone alleviates DOX-induced cardiotoxicity in mice and NRCMs

To investigate the role of idebenone in DOX-induced cardiotoxicity, we established an acute myocardial injury model by intraperitoneal DOX injection (15 mg/kg). Intragastrically, mice were administered idebenone (200 mg/kg) or normal saline once a day for 7 days before and after DOX treatment (Fig. 1A). As shown in Fig. 1B, idebenone treatment effectively inhibited DOX-induced cardiac dysfunction in mice, improving cardiac function indicators such as LVEF, LVFS, and LVESd. Meanwhile, the body weight of DOX-treated mice continued to decrease over time, and HW/TL was significantly reduced, which was prevented by idebenone treatment (Fig. 1C and D). More importantly, idebenone therapy significantly improved the survival rate of DOX administration mice (Fig. 1E). To assess myocardial morphology and cardiac fibrosis, we stained the heart paraffin sections with H&E and PSR. Results showed that mice treated with DOX had smaller hearts, a more disordered myocardium, and more perivascular and interstitial fibrosis than those treated with saline (Fig. 1F−H). The above pathological changes were significantly improved after idebenone administration. Further study showed that idebenone significantly down-regulated *Nppa* and *Nppb* mRNA levels (Fig. 1I and J), and reduced LDH in DOX-treated hearts (Fig. 1K). However, mice treated with or without idebenone did not differ significantly in heart rate (Fig. 1B).

Moreover, to assess the safety of idebenone, we observed the effects of idebenone on the mice's heart, and the results showed that idebenone at 0−400 mg/kg didn't induce cardiac injury (Fig. S1B). Additionally, no mice died in each idebenone-treated group. Then, we compared the serum ALT and CR levels between saline- and idebenone-treated mice, and the results showed no significant difference, along with the H&E stainings for the liver and kidney (Figs. S1C and S1D). Idebenone could significantly inhibit increased serum ALT and CR levels induced by DOX (Fig. S1D). Notably, we found that idebenone also reduced DOX-induced cardiac apoptosis (Supporting Information Figs. S2A and S2B).

For NRCMs experiments, we first examined the cytotoxic and efficacy of idebenone at different doses. As shown in Fig. 2A, CCK-8 assay results indicated that idebenone had no significant toxic effect on NRCMs at lower doses, only affecting cardiomyocyte viability at a higher dose of 100 μmol/L. More importantly, idebenone treatment markedly improved the cell viability of DOX-treated cardiomyocytes and we selected 5 μmol/L idebenone for subsequent experiments, as it improved the viability of NRCMs the most (Fig. 2B). All data indicate that idebenone could attenuate cardiac injury caused by DOX *in vivo* and *in vitro*.

3.2. Idebenone inhibits ROS overload-mediated ferroptosis in DOX-induced cardiotoxicity

It has been acknowledged that excessive ROS accounts for DOX-induced cardiac injury and previous studies demonstrate that idebenone has a potent antioxidant ability; thus, we detected ROS levels in mice hearts and NRCMs. We used DHE staining to detect ROS in heart-frozen sections. As shown in Fig. 2D, cardiac ROS levels were significantly elevated after DOX treatment, which was improved by idebenone. Consistently, the immunohistochemistry of cardiac paraffin sections revealed that idebenone downregulated 4-HNE levels in DOX-challenged cardiomyocytes. Following the results in mice hearts, DCFH-DA staining and Flow Cytometry of NRCMs also proved that idebenone treatment reduced ROS accumulation induced by DOX (Fig. 2E and F). Intracellular ROS overload has been proposed that may induce ferroptosis, a novel cell death program characterized by iron-dependent membrane

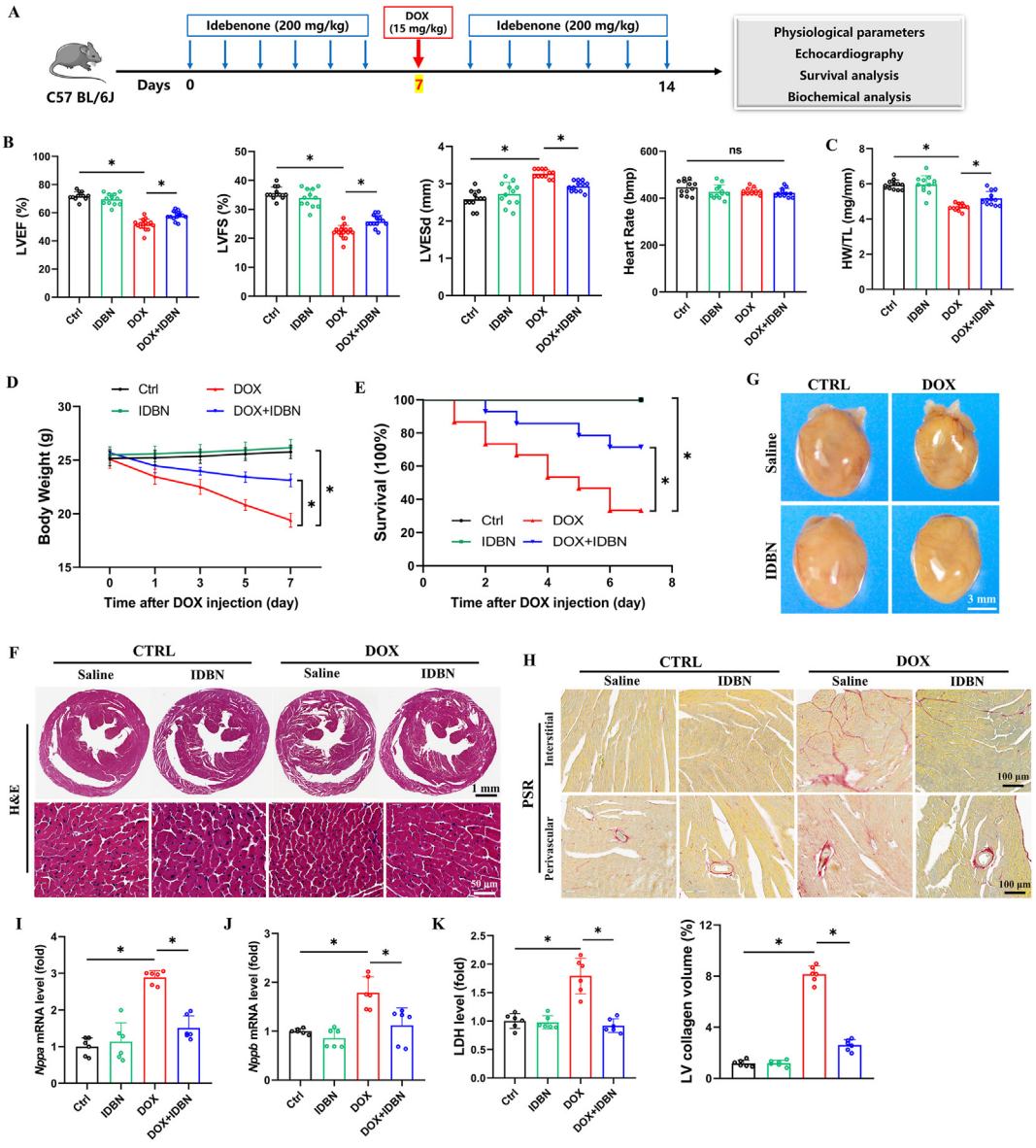

Figure 1 Idebenone attenuates DOX-induced cardiotoxicity and cardiac remodeling *in vivo*. (A) Flow chart of the experimental protocol *in vivo*. (B) Analyses of LVEF, LVFS, LVESd and Heart rate, $n = 12$. (C) Analyses of heart weight/tibia length (HW/TL) ratio, $n = 12$. (D) Body weight alterations after DOX (15 mg/kg) injection. (E) Analyses of survival in each group, $n = 12$. (F) Representative images of H&E staining (scale bar = 1 mm for 10× magnification; scale bar = 50 μm for 400× magnification, $n = 6$). (G) Representative pictures of the gross heart morphology (scale bar = 3 mm, $n = 6$). (H) Representative images of PSR staining (scale bar = 100 μm, $n = 6$), and quantification of cardiac fibrosis by PSR staining. (I, J) Relative cardiac mRNA levels of *Nppa* and *Nppb*, normalized to β-actin, $n = 6$. (K) Cardiac LDH levels, $n = 6$. Data are presented as the mean ± SEM, with each point representing an independent experiment. $^*P < 0.05$ *versus* the matched group.

lipid peroxidation affecting oxidative stress-induced cardiac injury in response to DOX. Then we explored whether idebenone could rescue DOX-induced myocardial injury by inhibiting cardiac ferroptosis *in vivo* and *in vitro*. As shown in Fig. 2G and H, idebenone reduced the protein and mRNA levels of the ferroptosis marker PTGS2 in DOX-induced cardiotoxicity. We further compared idebenone's efficacy in inhibiting ferroptosis with the ferroptosis inhibitors Ferrostatin-1 (Fer-1) and deferoxamine (DFO). As shown in Supporting Information Fig. S3, idebenone inhibits ferroptosis similarly to Fer-1 and DFO in the presence of DOX. More importantly, we found idebenone could significantly attenuate MDA levels, a hallmark of lipid peroxidation, in hearts and NRCMs (Fig. 2C). Consistent with the MDA results, idebenone significantly rescued DOX-induced downregulation of SOD, GSH, and GSH-Px levels (Fig. S2C−S2E). To verify lipid ROS products further, C11-BODIPY, a membrane-integrated dye that changes color from red to green when oxidized, was used in this experiment. DOX significantly increased lipid ROS levels in NRCMs, which was effectively reversed by idebenone (Fig. 2I). Additionally, we used JC-1 staining to evaluate DOX-induced mitochondrial injury, an early sign of ferroptosis[19]. As expected, the results revealed that idebenone reduced abnormal mitochondrial membrane potential caused by DOX (Fig. 2J). We next observed mitochondria in each group of mice's hearts using

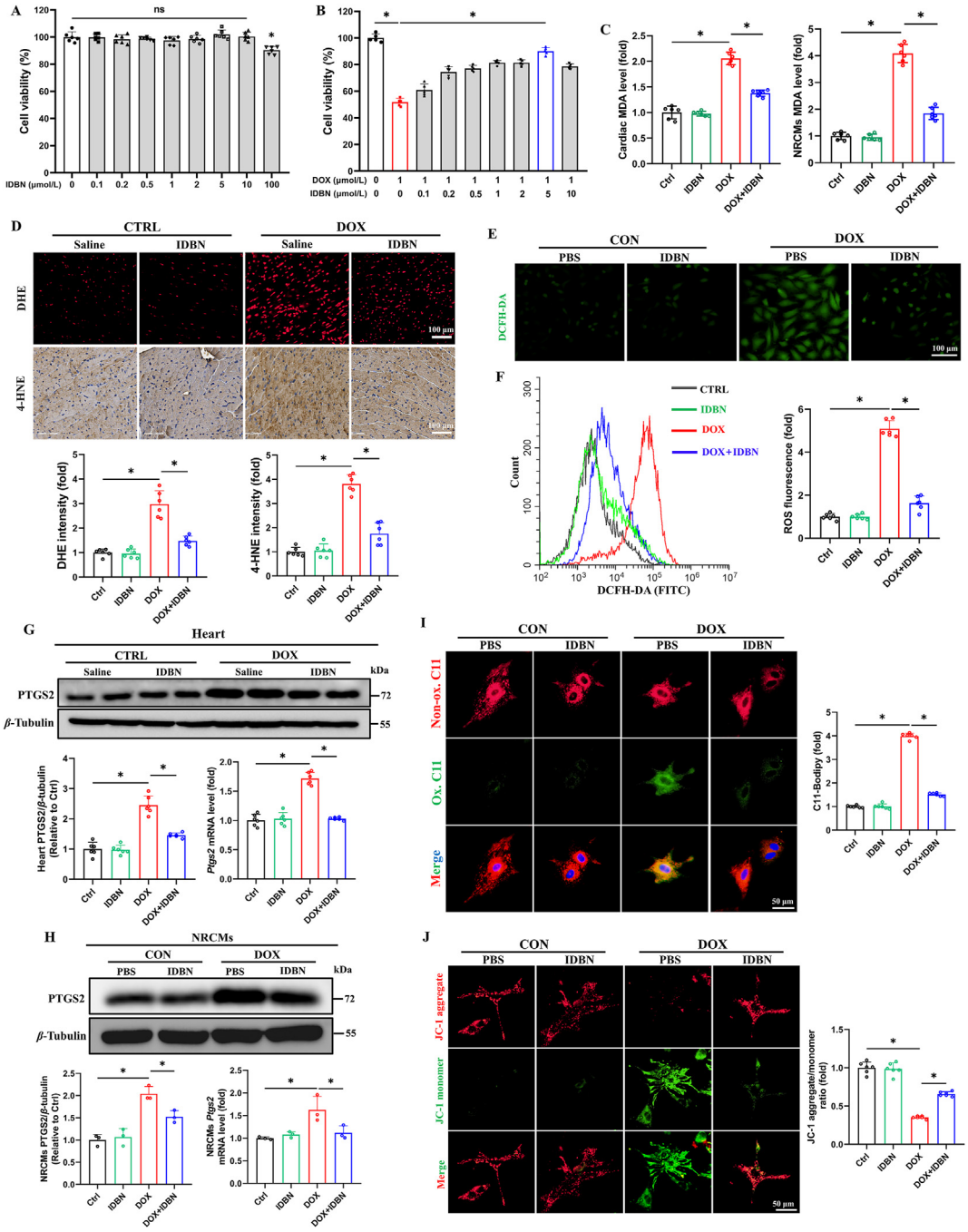

Figure 2 Idebenone protects against DOX-induced cardiotoxicity by inhibiting ROS overload-induced ferroptosis. (A) Cell viability after treatment with different idebenone doses in NRCMs, measured by CCK8, $n = 6$. (B) Cell viability after treatment with different idebenone doses in the presence of DOX (1 μmol/L) in NRCMs, measured by CCK8, $n = 6$. (C) Relative MDA levels in mice hearts and NRCMs, $n = 6$. (D) Representative images and quantification of DHE and 4-HNE staining in heart sections (scale bar = 100 μm, $n = 6$). (E) Representative images of DCFH-DA staining in NRCMs, and quantification of ROS density (scale bar = 100 μm, $n = 6$). (F) Flow cytometry analysis of FITC-ROS in each group ($n = 6$). (G) Representative Western blotting images of PTGS2, and quantitative analysis were performed using image lab software; relative *Ptgs2* mRNA levels, normalized to β-actin in indicated mice groups, $n = 6$. (H) Representative Western blotting images of PTGS2 and β-tubulin in NRCMs, and quantitative analysis were performed using image lab software, and relative *Ptgs2* mRNA levels in NRCMs, normalized to β-actin, $n = 3$. (I) Representative images of C11-BODIPY 581/591 staining in NRCMs, and quantification of C11-BODIPY levels (scale bar = 50 μm, $n = 6$). (J) Representative images of JC-1 staining in NRCMs, and quantification of JC-1 aggregate/monomer ratio (scale bar = 50 μm, $n = 6$). Data are presented as the mean ± SEM, and each point represents an independent culture. $^*P < 0.05$ *versus* the matched group.

transmission electron microscopy. As a result, mitochondria in DOX-treated mice were disorganized and severely distorted, and mitochondrial cristae were disrupted, which was notably reversed by idebenone (Supporting Information Fig. S4). The above data suggest that idebenone attenuates DOX-induced cardiotoxicity by inhibiting lipid ROS accumulation-mediated ferroptosis.

3.3. Idebenone alleviates ROS-induced ferroptosis by regulating iron metabolism in DOX-treated groups

Ferroptosis is iron-dependent and usually triggered by iron metabolism disturbances like intracellular iron overload or excessive Fe^{2+} accumulation, which could produce ROS. Prussian blue staining showed that DOX increased cardiac iron levels, which was attenuated by idebenone treatment (Fig. 3A). More importantly, FerroOrange staining of cardiomyocytes confirmed that idebenone significantly alleviated Fe^{2+} accumulation induced by DOX, suggesting the Fenton reaction, a process of reacting Fe^{2+} with H_2O_2 to produce highly reactive hydroxyl radicals, could be inhibited by idebenone (Fig. 3B). We further examined the protein expression levels related to iron metabolism in heart tissue and NRCMs. As shown in Fig. 3C and D, TFR1 was upregulated, and FTH1 and FTL were downregulated in the DOX treatment group, which were reversed by idebenone. And TFR1 immunofluorescence staining further confirmed that idebenone improved DOX-induced iron metabolism disorder (Fig. 3E). As a

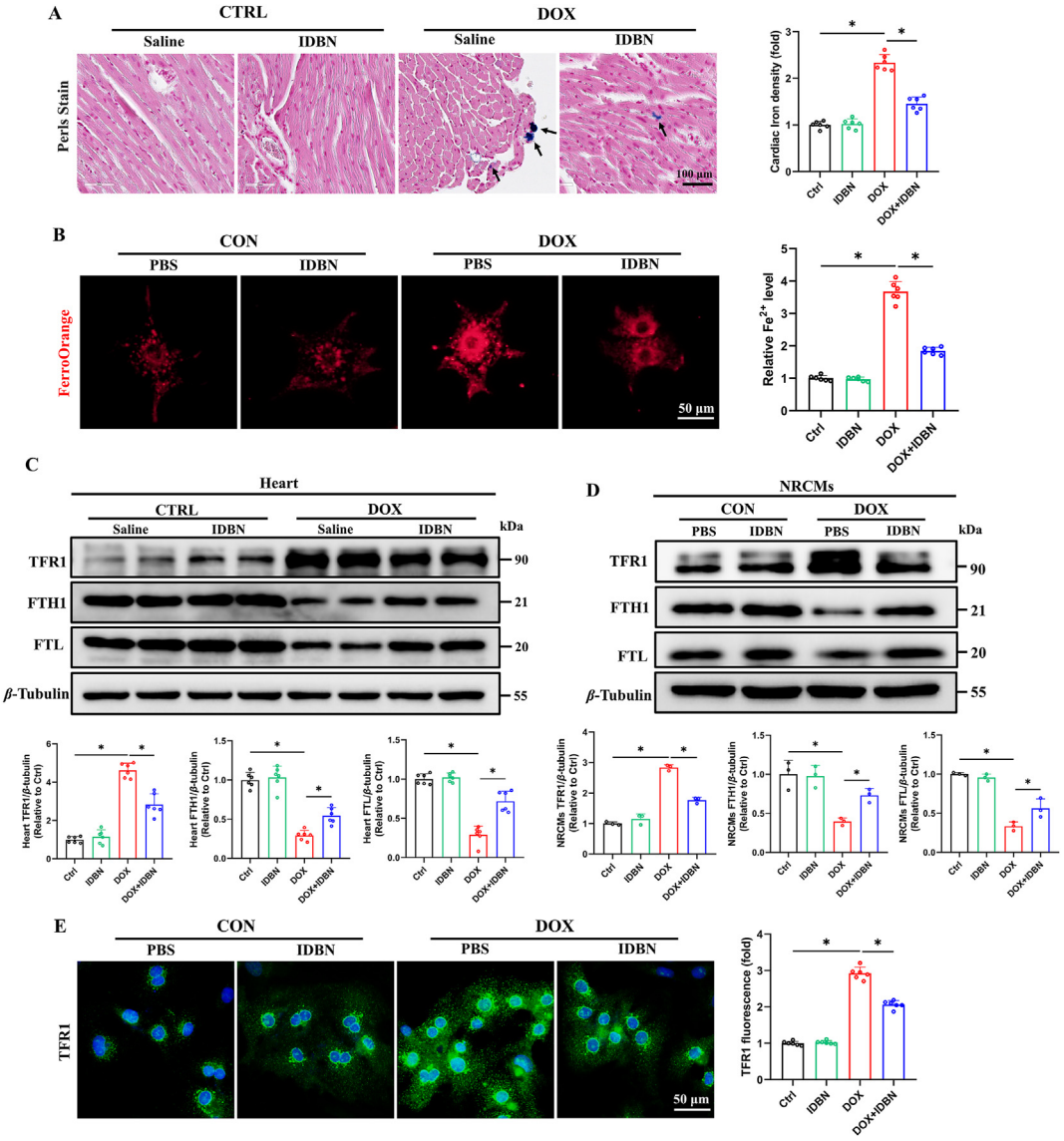

Figure 3 Idebenone inhibits ROS-induced ferroptosis by regulating iron metabolism in DOX-induced cardiotoxicity. (A) Representative images of Prussian blue staining in heart sections and quantification of cardiac iron density (scale bar = 100 μm, $n = 6$). (B) Representative images of FerroOrange staining in NRCMs, and quantification of Fe^{2+} levels (scale bar = 50 μm, $n = 6$). (C) Representative Western blotting images of TFR1, FTH1, FTL, and β-tubulin in the heart, and quantitative analysis were performed using image lab software, $n = 6$. (D) Representative Western blotting images of TFR1, FTH1, FTL, and β-tubulin in NRCMs, and quantitative analysis were performed using image lab software, $n = 3$. (E) Representative images of TFR1 immunofluorescence staining in NRCMs and quantification of TFR1 fluorescence density (scale bar = 50 μm, $n = 6$). Data are presented as the mean ± SEM, and each point represents an independent culture. $^*P < 0.05$ *versus* the matched group.

whole, these data demonstrated that idebenone inhibits Fe^{2+} accumulation and Fenton reaction in DOX-induced cardiotoxicity, thus alleviating ROS-induced ferroptosis.

3.4. *Idebenone inhibits ferroptosis by interacting with FSP1 in Dox-mediated cardiotoxicity*

Although idebenone has been identified as a ferroptosis inhibitor, the mechanism for its anti-ferroptosis remains unclear, especially in DOX-mediated cardiotoxicity. To further explore the specific mechanism of idebenone inhibiting DOX-induced ferroptosis, we detected the critical proteins mediating ferroptosis in heart tissue and NRCMs with different treatments. We examined the expression of proteins GPX4 and FSP1, two antioxidants inhibiting ferroptosis. As expected, idebenone treatment significantly ameliorated DOX-induced downregulation of GPX4, FSP1 (Fig. 4A and B). And immunofluorescent and immunohistochemistry staining of heart sections showed that idebenone significantly restored FSP1 levels in DOX-induced hearts (Fig. 4C and D).

To further explore the anti-ferroptosis mechanism of idebenone, we examined the molecular docking of the interaction between idebenone and key protein targets in the ferroptosis signaling pathway. Previous studies have shown that FSP1, DHODH, and GPX4 are critical targets for ferroptosis antioxidants. And TFR1, FTH1, FPN, and DMT1 are essential proteins that regulate iron metabolism homeostasis in cells. Alternatively, ACSL4 and SLC7A11 have been reported to be critical in regulating cardiac ferroptosis. Thus, to verify the interaction of idebenone with ferroptosis essential proteins, we performed batch molecular docking of idebenone with FSP1, GPX4, DHODH, TFR1, FTH1, FPN, DMT1, ACSL4, and SLC7A11 using Autodock vina. Interestingly, idebenone had the highest binding energy (−8.2 kcal/mol) to FSP1 (Supporting Information Fig. S5A). Using Pymol further to analyze the binding form of idebenone and FSP1, we observed that idebenone forms a binding pocket with FSP1 (Fig. 4E). Cellular Thermal Shift Assay (CESTA) further confirms that idebenone binds to FSP1 proteins but not GPX4 (Fig. 4F). To further determine the interaction of idebenone with FSP1, Biolayer Interferometry (BLI) were conducted *in vitro*. As shown in Fig. 4G and Fig. S5B, idebenone had an obvious binding signal to the FSP1 protein, high affinity and strong concentration dependence, K_D = 8.4 μmol/L. The above data show that idebenone can stably bind to FSP1 to affect protein function or post-translational modification. Previous studies have shown that FSP1, a ferroptosis defence system independent of the GPX4 system, is a CoQ_{10} oxidoreductase that prevents lipid peroxidation by reducing CoQ_{10} to $CoQ_{10}H_2$[10,20]. Therefore, we detected CoQ_{10} and $CoQ_{10}H_2$ levels in mice' heart tissue. As shown in Fig. 4H and I, both CoQ_{10} and $CoQ_{10}H_2$ were significantly down-regulated in DOX-induced myocardial tissue, and the proportion of $CoQ_{10}H_2$ down-regulated was much higher. By contrast, idebenone protection reversed this trend. More importantly, idebenone significantly improved the ratio of $CoQ_{10}H_2/CoQ_{10}$, indicating that idebenone enhanced the ability of FSP1 to reduce CoQ_{10} (Fig. 4J).

3.5. *FSP1 deficiency abolishes idebenone's benefit in DOX-induced ferroptosis*

To further determine whether idebenone alleviates DOX-induced cardiotoxicity through regulating FSP1, we constructed a cardiomyocyte model with FSP1 knockdown by si-RNA. First, we verified the efficiency of knocking down FSP1 after the transfection of si-FSP1 into NRCMs. Compared with the control group, Western Blot and RT-PCR showed that FSP1 protein and mRNA levels were reduced by 5−7 times after si-FSP1 transfection in NRCMs (Supporting Information Fig. S6A−S6C). Next, we found that FSP1 knockdown significantly enhanced DOX-induced decline in cardiomyocyte viability and abolished the benefit of idebenone treatment (Fig. 5A). Considering that idebenone attenuates DOX-induced cardiotoxicity *via* inhibition of ferroptosis, we examined markers of ferroptosis following si-FSP1. As shown in Fig. 5B−D, MDA levels, *Ptgs2* mRNA and protein levels were upregulated after DOX-treated and further upregulated after si-FSP1 transfection. And FSP1 knockdown abolished the ability of idebenone to scavenge lipid peroxidation (Fig. 5B−D). Next, we further examined iron metabolism, and the results showed that si-FSP1 aggravated DOX-induced increase in the labile iron pool. More specifically, the improvement effect of idebenone on iron metabolism was abolished by FSP1 knockdown (Fig. 5D and E). Intracellular ROS staining, flow cytometry and C11-BODIPY staining further confirmed that si-FSP1 abrogated idebenone inhibition of DOX-induced ferroptosis (Fig. 5E−G).

We further investigated whether FSP1 inactivation (iFSP1, a selective inhibitor of FSP1) abolished the effect of idebenone on inhibiting DOX-induced ferroptosis. As shown in Fig. 6A−D, DOX or the ferroptosis inducer Erastin significantly upregulated the protein expression levels of PTGS2 and TFR1, decreased the expression of FTH1, and superposition had an enhanced effect. Consistent with the si-FSP1 results, idebenone's inhibitory effect on ferroptosis was counteracted by iFSP1 treatment. ROS and C11-BODIPY staining, and MDA levels further confirmed the inhibition of FSP1 reductase activity, counteracting the effect of idebenone on scavenging DOX-induced lipid peroxidation (Fig. 6E−H). Interestingly, iFSP1 inhibited the reduction ratio of $CoQ_{10}H_2/CoQ_{10}$ (Fig. 6I). Therefore, we used 4-chlobenzoic acid (4-CBA) treatment to inhibit CoQ_{10} biogenesis[21]. 4-CBA significantly enhanced DOX-induced ferroptosis compared with controls and was not rescued by idebenone treatment (Fig. 6J).

Overall, these data revealed that FSP1 inhibition significantly enhanced DOX-induced ferroptosis sensitivity. More critically, FSP1 ablation and inhibition of enzyme activity abolished the rescue effect of idebenone against DOX-induced cardiotoxicity. On the other hand, inhibition of CoQ_{10} biosynthesis also abolished the protective effect of idebenone. Thus, inhibition of the FSP1 greatly abolished idebenone's inhibitory effect in DOX-induced ferroptosis.

3.6. *Overexpressed FSP1 in cardiomyocytes attenuates DOX-induced cardiotoxicity by inhibiting cardiac ferroptosis*

The above experimental data indicated that idebenone inhibited DOX-induced cardiotoxicity by up-regulating FSP1. Therefore, to determine whether FSP1 overexpression protects against DOX-induced cardiotoxicity, we constructed an AAV9-FSP1 vector specifically overexpressing cardiomyocytes (Supporting Information Fig. S7A). Four weeks after tail vein injection of AAV9-FSP1 in mice, Western blotting and immunofluorescence staining showed that FSP1 expression was significantly upregulated in the heart (Fig. S7B and S7C). Next, we evaluated cardiac function and cardiac pathologic remodeling in each group of mice. As shown in Fig. 7A and C, echocardiography revealed that FSP1 overexpression in cardiomyocytes significantly alleviates DOX-induced cardiac dysfunction. And Vevo Strain analysis found

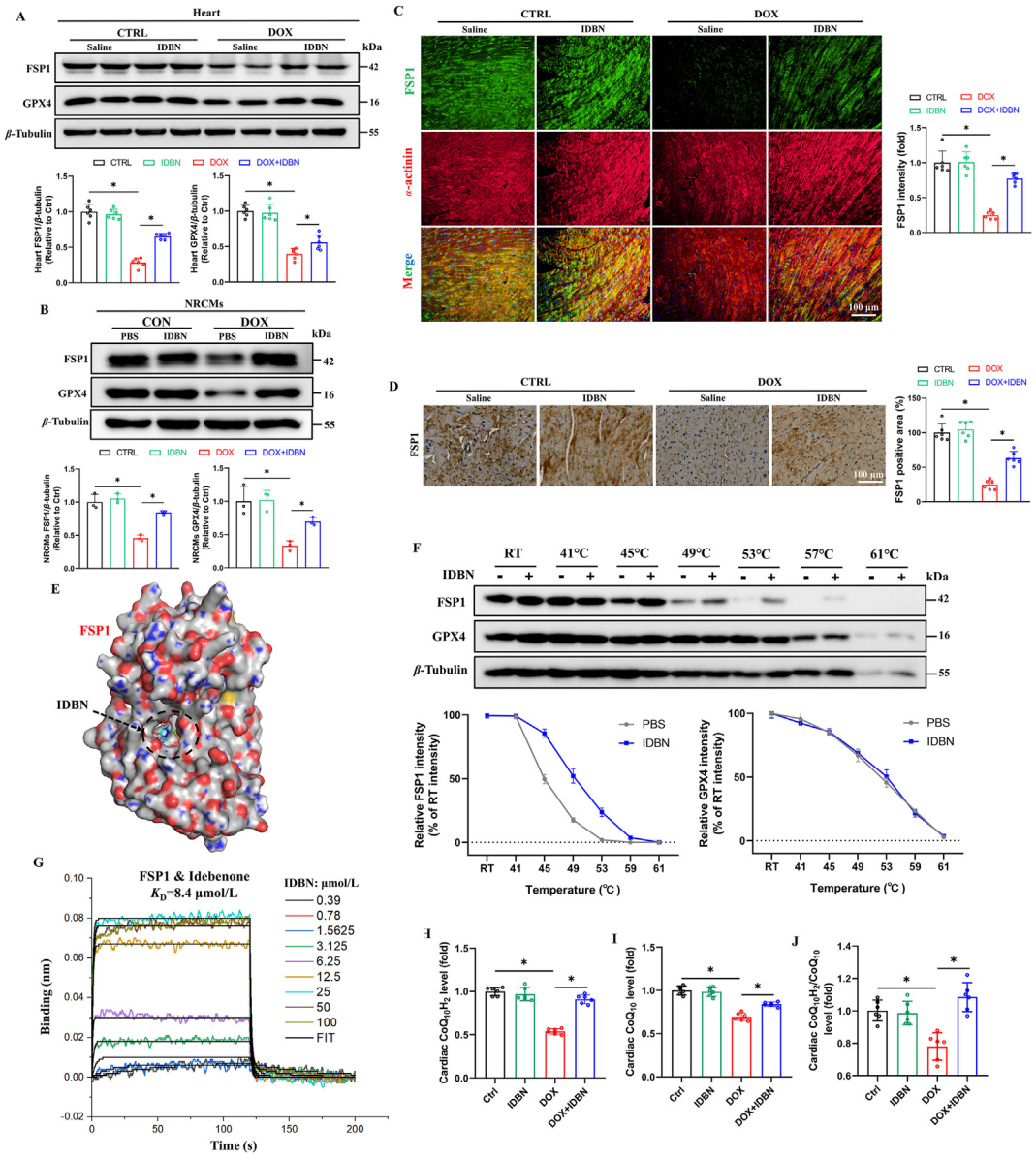

Figure 4 Idebenone interacts with the FSP1 protein and regulates iron metabolism. (A) Representative Western blotting images of FSP1, GPX4, and β-tubulin in the heart, and quantitative analysis were performed using image lab software, $n = 6$. (B) Representative Western blotting images of FSP1, GPX4, and β-tubulin in NRCMs, and quantitative analysis were performed using image lab software, $n = 3$. (C) Representative images of FSP1 and α-actinin immunofluorescence staining in heart sections and quantification of FSP1 fluorescence density (scale bar = 100 μm, $n = 6$). (D) Representative images of FSP1 immunohistochemical staining in heart sections and quantification of FSP1 positive area (scale bar = 100 μm, $n = 6$). (E) The surface map of the binding conformation of idebenone to FSP1 protein by Autodck Vina, and the docking pocket is outlined by a dotted line. (F) Representative Western blotting images of FSP1, GPX4 and β-tubulin of thermal shift assay in NRCMs lysate treated with or without IDBN, $n = 3$. (G) A real-time kinetic binding sensorgram is shown for different IDBN concentrations ranging from 0.39 to 100 μmol/L. Response (nm) represents the optical thickness of the SA biosensor layer. (H–J) Cardiac CoQ_{10} and $CoQ_{10}H_2$ levels and $CoQ_{10}H_2/CoQ_{10}$ ratio, were measured by Elisa, $n = 6$. Data are presented as the mean ± SEM, and each point represents an independent experiment. *$P < 0.05$ *versus* the matched group.

that FSP1 overexpression improved left ventricular Global longitudinal strain (GLS) in DOX-treated mice (Fig. 7D). More importantly, AAV9-FSP1 treatment significantly improved survival rates compared to DOX-treated mice (Fig. 7B). Furthermore, pathological staining and gross sampling results showed that AAV9-FSP1 ameliorated DOX-induced loss in heart weight, HW/TL, and body weight, as well as cardiomyocyte disorder and myocardial fibrosis (Fig. 7E, F and Fig. S7D). We next examined the effect of FSP1 overexpression on DOX-induced cardiac ferroptosis. As expected, FSP1 overexpression significantly improved DOX-induced disturbance of lipid peroxidation and iron metabolism (Fig. 7G–J). As a result, FSP1 overexpression protects against DOX-induced cardiotoxicity by suppressing ferroptosis.

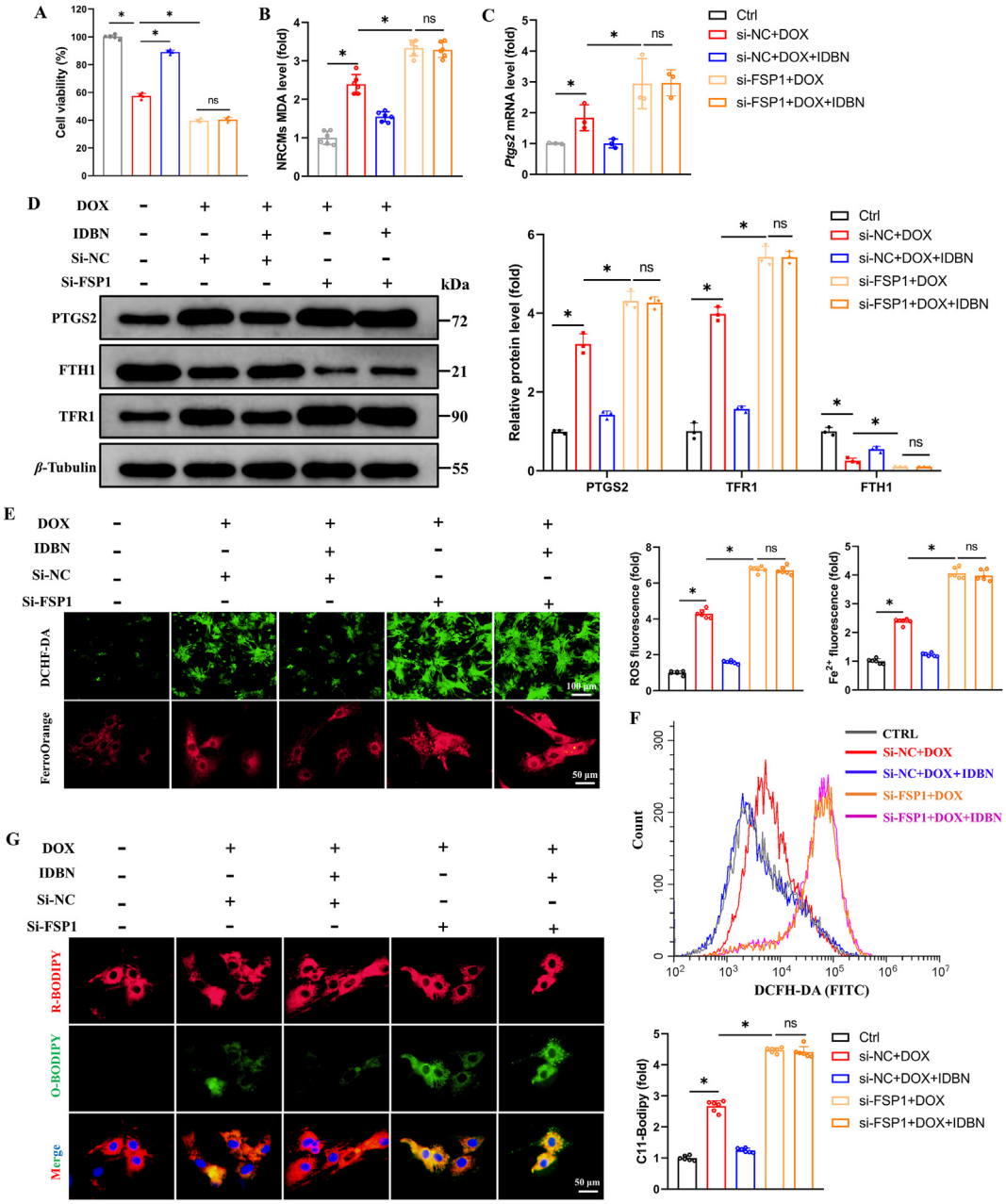

Figure 5 FSP1 deficiency abolishes idebenone's benefit in DOX-induced ferroptosis. (A) Cell viability measured by CCK8 in each group, $n = 6$. (B) MDA levels in NRCMs, $n = 6$. (C) Relative mRNA levels of *Ptgs2* in NRCMs, normalized to β-actin, $n = 3$. (D) Representative Western blotting images of PTGS2, TFR1, FTH1, and β-tubulin in NRCMs, and quantitative analysis were performed using image lab software, $n = 3$. (E) Representative images of DCFH-DA and FerroOrange staining in NRCMs, and quantification of ROS density and Fe^{2+} levels (upper scale bar = 100 μm, below scale bar = 50 μm, $n = 6$). (F) Flow cytometry analysis of FITC-ROS in each group, $n = 6$. (G) Representative images of C11-BODIPY 581/591 staining in NRCMs, and quantification of C11-BODIPY levels (scale bar = 50 μm, $n = 6$). Data are presented as the mean ± SEM, and each point represents independent cultures. $^*P < 0.05$ *versus* the matched group.

3.7. Idebenone regulates FSP1 protein degradation through the ubiquitin−proteasome pathway

Our previous results showed that idebenone significantly increased the protein level of FSP1 (Fig. 4A and B), which inhibited Fe^{2+} accumulation (Fig. 3C and D) and enhanced the conversion of CoQ_{10} to $CoQ_{10}H_2$ (Fig. 4J), thereby inhibiting DOX-induced ferroptosis. To further explore how idebenone regulates FSP1, we detected *Fsp1* mRNA level. As shown in Fig. 8A, idebenone treatment did not influence the transcriptional level of Fsp1 (Fig. 8A). Based on the Autodock analysis, CESTA, BLI analysis above (Fig. 4E−G) and *Fsp1* mRNA results, we hypothesize that idebenone may modulate FSP1 protein level *via* post-translational modification. Previous studies have shown that the protein abundance of FSP1 can be regulated by the polyubiquitination−proteasome pathway[22,23]. We first treated NRCMs with either the protein biosynthesis inhibitor cycloheximide (CHX) or the proteasome inhibitor MG-132. As shown in Fig. 8B, CHX significantly enhanced DOX-induced downregulation

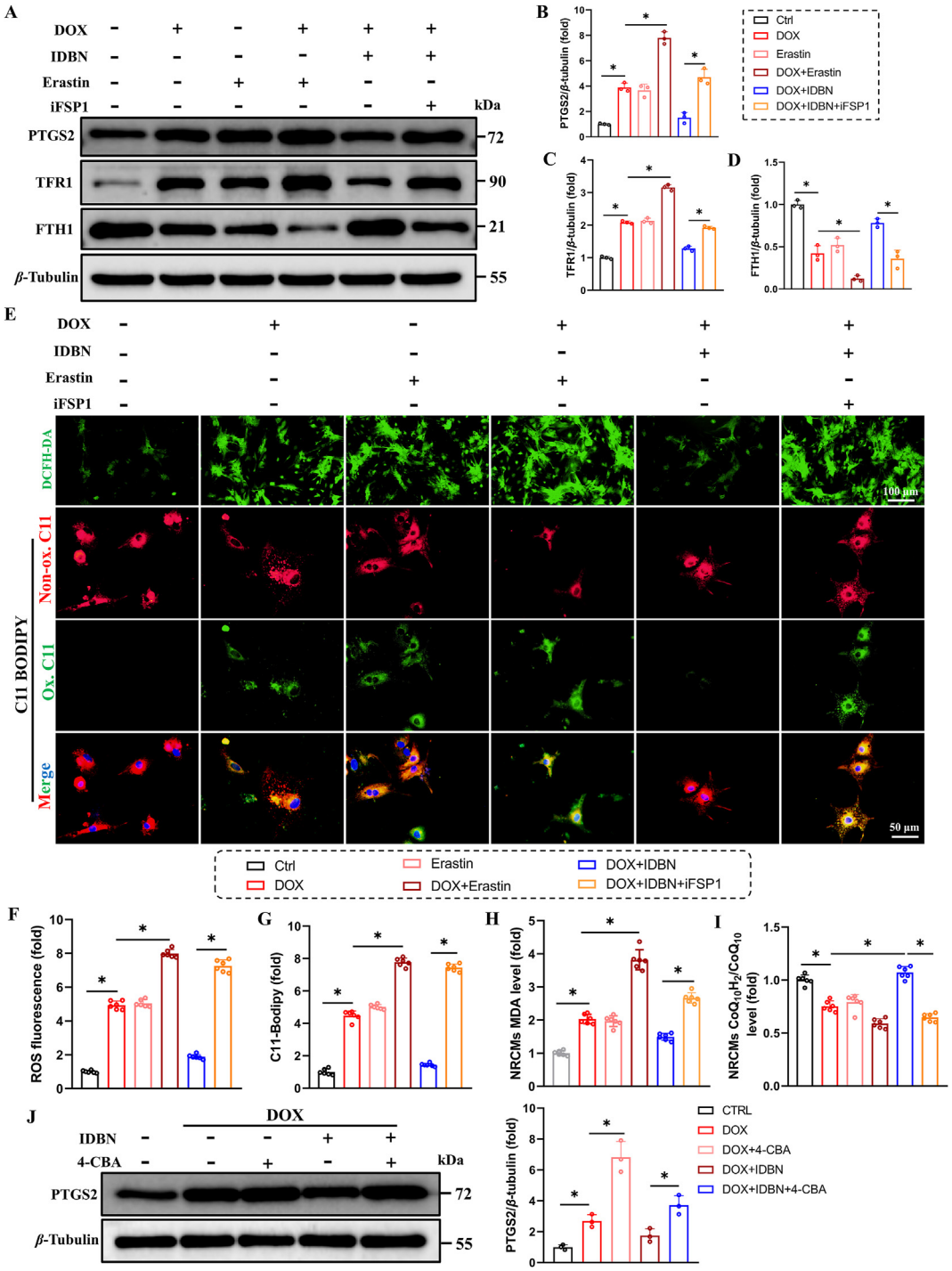

Figure 6 FSP1 activity and CoQ10 synthesis inhibition abolished idebenone's benefit in DOX-induced ferroptosis. (A−D) Representative Western blotting images of PTGS2, TFR1, FTH1, and β-tubulin in NRCMs, and quantitative analysis were performed using image lab software, $n = 3$. (E−G) Representative images of DCFH-DA and C11-BODIPY 581/591 staining in NRCMs, and quantification of ROS density and C11-BODIPY levels (upper scale bar = 100 μm, below scale bar = 50 μm, $n = 6$). (H) MDA levels in NRCMs, $n = 6$. (I) $CoQ_{10}H_2/CoQ_{10}$ ratio in NRCMs, measured by Elisa, $n = 6$. (J) Representative Western blotting images of PTGS2 in NRCMs, and quantitative analysis were performed using image lab software, $n = 3$. Data are presented as the mean ± SEM, and each point represents an independent culture. $^*P < 0.05$ *versus* the matched group.

of FSP1 protein levels, an effect partially attenuated by idebenone. More critically, MG-132 treatment upregulated the protein level of FSP1 in DOX-treated NRCMs, whereas idebenone combined treatment did not affect the FSP1 expression level, suggesting idebenone regulates FSP1 level by ubiquitination (Fig. 8C). On the other hand, considering autophagy as another key pathway for protein degradation, we investigated whether idebenone affects FSP1 protein levels through autophagy. As shown in Supporting Information Fig.

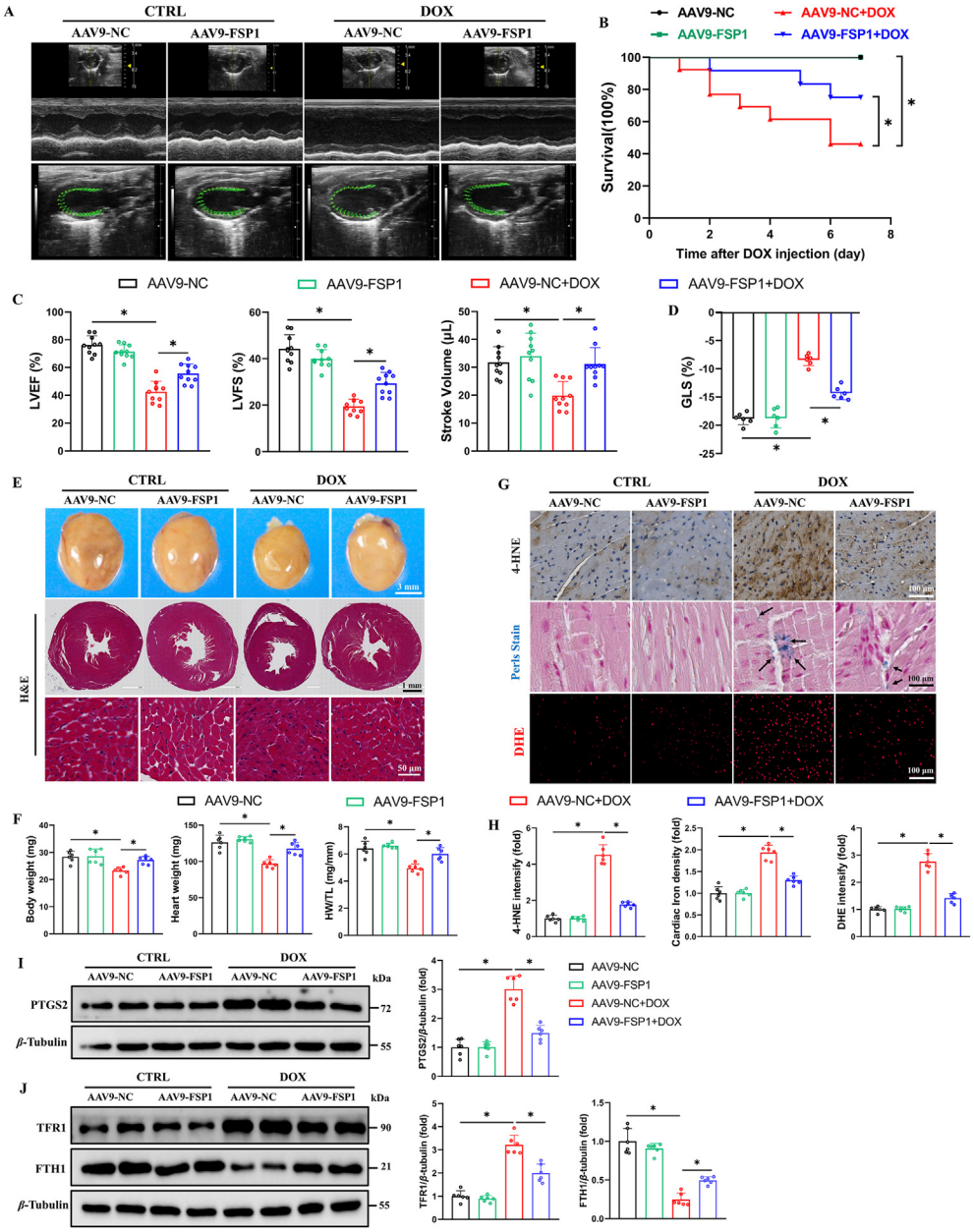

Figure 7 FSP1 overexpression alleviates DOX-induced cardiotoxicity by inhibiting ferroptosis. (A) Representative images of M-mode and ventricular wall motion echocardiography, $n = 10$. (B) Analyses of survival in each group. (C) Analyses of LVEF, LVFS, Stroke volume, Heart rate, $n = 10$. (D) Analyses of Global longitudinal strain (GLS) by Vevo Strain, $n = 6$. (E) Representative picture of the gross heart morphology (scale bar = 3 mm), and H&E staining (scale bar = 1 mm for 10 × magnification; scale bar = 50 μm for 400 × magnification, $n = 6$). (F) Analyses of heart weight, heart weight/tibia length (HW/TL) ratio and body weight, $n = 6$. (G) Representative images of 4-HNE, Prussian blue and DHE staining in heart sections (scale bar = 100 μm, $n = 6$). (H) Quantitatively analyzed 4-HNE, cardiac iron density and DHE intensity, $n = 6$. (I, J) Representative Western blotting images of PTGS2, TFR1, FTH1 and β-tubulin in hearts, and quantitative analysis were performed using image lab software, $n = 6$. Data are presented as the mean ± SEM, and each point represents an independent experiment. *$P < 0.05$ *versus* the matched group.

S8A–S8D, DOX activates autophagy in cardiomyocytes, but idebenone treatment does not affect autophagic flux levels. Next, we examined the effect of idebenone on FSP1 protein degradation under autophagy inhibition or activation. The results show that idebenone further upregulated FSP1 protein levels treated with autophagy inhibitor 3-MA or CQ in DOX-treated NRCMs, and idebenone treatment reversed the down-regulation of FSP1 levels caused by stimulation of the autophagy activator RAPA but did not affect autophagic flux, suggesting that idebenone does not regulate the proteostasis of FSP1 through autophagy (Supporting Information Fig. S9A–S9D). Then, we detected the expression levels of ubiquitinated proteins in cardiac tissues and NRCMs to evaluate idebenone's regulative effect on FSP1 protein abundance. The data confirmed that DOX treatment significantly upregulated ubiquitin protein expression, which was reversed by idebenone (Fig. 8D and E). Furthermore, we detected FSP1 expression at different time points under DOX

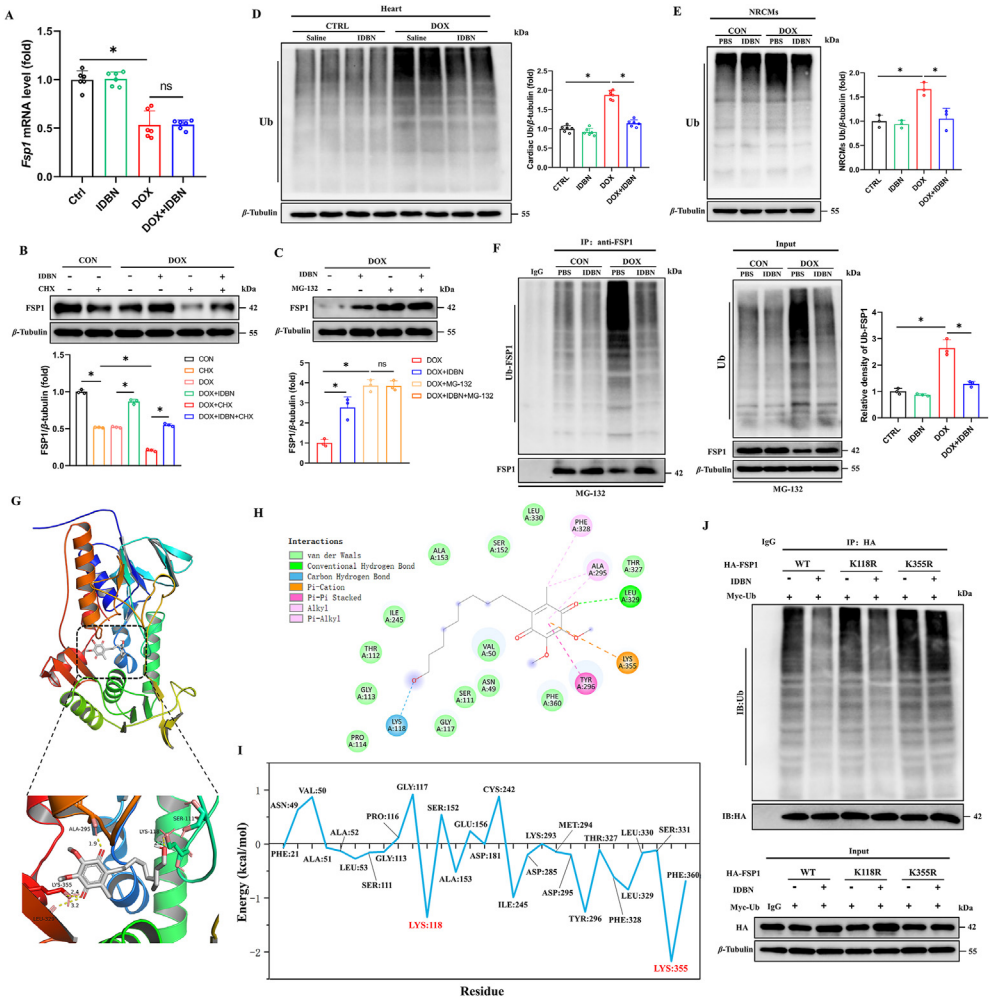

Figure 8 Idebenone influences FSP1 protein degradation *via* the ubiquitin−proteasome pathway. (A) Relative mRNA levels of *Fsp1* in hearts, normalized to β-actin, $n = 6$. (B, C) Representative Western blotting images of FSP1 and β-tubulin in NRCMs, and quantitative analysis were performed using image lab software, $n = 3$. (D, E) Representative Western blotting images of ubiquitin and β-tubulin in hearts and NRCMs, and quantitative analysis were performed using image lab software, $n = 3$−6. (F) Ubiquitination of FSP1 (Ub-FSP1) was detected by immunoprecipitation in NRCMs, and subsequently quantitatively analyzed by image lab software, $n = 3$. (G) The cartoon diagram of the binding conformation of idebenone and FSP1 protein shows the site of interaction and the length of the hydrogen bond. (H) Molecular dynamics simulation analysis of the interaction between idebenone and FSP1 in the docking pocket. (I) Analysis of the energy contribution of key amino acid residues to the binding pocket. (J) Representative Western blot of 293T cells transfected with Myc-Ub and HA-FSP1-WT or FSP1-K118R or FSP1-K355R mutants immunoprecipitation with anti-HA antibody, and tested by ubiquitination, HA-tagged and β-tubulin antibodies, $n = 3$. Data are presented as the mean ± SEM, and each point represents an independent experiment. $^*P < 0.05$ *versus* the matched group.

stimulation in the presence of idebenone or PBS. The results showed that idebenone could slow down FSP1 degradation under DOX stimulation (Supporting Information Fig. S10A−S10C). More importantly, Co-IP strongly confirmed that idebenone significantly down-regulated the protein level of ubiquitination-bound FSP1, thereby inhibiting the ubiquitin−proteasome degradation pathway of FSP1 (Fig. 8F). Autodock and Pymol analysis suggested that idebenone has stable hydrogen bonding interactions with FSP1 at Ser111/Lys118/Als295/Lys355 (Fig. 8G). Further molecular dynamics simulations revealed the energy changes, electrostatic potential energy, and hydrophobicity of idebenone and FSP1 binding in a stable conformation (Supporting Information Fig. S11). The results indicated the intermolecular interaction form of the binding pocket of FSP1 and idebenone with an affinity energy of −24.00 kcal/mol (Fig. 8H). Further analytical calculations showed that the binding free energy contribution of LYS118 and LYS355 was the largest (Fig. 8I). Considering that ubiquitin binding sites are generally lysine residues, we constructed FSP1-WT, FSP1-K118 and FSP1-K355 site mutation plasmids. Plasmid transfection and Co-IP in HEK 293T cells showed that idebenone regulates FSP1 ubiquitination and degradation by affecting the K355 site (Fig. 8H).

In summary, the above data support the hypothesis that idebenone inhibits the ubiquitin−proteasome pathway of FSP1 by reducing the binding of FSP1-K355 to ubiquitin molecules, thereby increasing the protein abundance of FSP1 and inhibiting DOX-induced ferroptosis and cardiotoxicity.

4. Discussion

The current clinical treatment for DOX-induced cardiotoxicity is limited, and it is urgent to find potential targets and drug treatments[24,25]. According to our study, we identified idebenone as a

potential therapeutic drug to protect against DOX-induced cardiotoxicity. We confirmed that idebenone improves cardiac function deterioration and survival in mice induced by acute DOX intraperitoneal injection. Mechanistically, we demonstrated that: (a) idebenone inhibits ferroptosis to protect against DOX-induced cardiotoxicity by reducing lipid peroxidation and iron overload in cardiomyocytes; (b) idebenone up-regulates FSP1 protein level and increases the ratio of $CoQ_{10}H_2/CoQ_{10}$ to inhibit DOX-induced ferroptosis; (c) idebenone blocks FSP1 ubiquitination by stable binding to FSP1, thereby reducing FSP1 degradation by the ubiquitin−proteasome pathway. Our study systematically elucidated the role of idebenone in DOX-induced cardiotoxicity and uncovered its specific mechanism, providing a potential strategy for treating patients with DOX-induced cardiotoxicity in clinical practice.

To date, there are limited drugs approved for the treatment of DOX-induced cardiac injury, and Dexrazoxane remains the sole clinical drug endorsed by the FDA for addressing DOX-induced cardiotoxicity. However, the efficacy of dexrazoxane may be mitigated by reduced chemotherapy sensitivity in cancer cells and aggravated myelosuppression, which curtails its utilization in treatment[26]. Idebenone was initially designed for neurological disorders such as Duchenne muscular dystrophy[12], Leber hereditary optic neuropathy[27], Alzheimer's disease[28], etc. Recent investigations suggest that idebenone can be extended to treat cardiovascular diseases such as atherosclerosis[14] and myocardial infarction[29]. Idebenone has a shorter lipophilic side chain that increases its solubility and membrane affinity, and the side chain also contains terminal hydroxyl groups to increase polarity[13]. A multicenter randomized double-blind controlled trial has confirmed that idebenone treatment was safe and well tolerated[12]. Our results also proved that idebenone at therapeutic doses had no adverse effect on liver or kidney function, nor did it have an acute toxic effect on the heart and cardiomyocytes. As a drug used in clinics, idebenone is cheap, easy to obtain, and has substantial advantages in clinical transformation.

DOX-induced cardiotoxicity is caused by a variety of cell death pathways. Fang et al.[4] revealed the contribution of ferroptosis, autophagy, apoptosis, necroptosis and other cell death pathways in DOX-induced cardiotoxicity, the results showed that ferroptosis plays the most critical role. And recent studies have identified ferroptosis as a critical mechanism of DOX-induced cardiotoxicity[4,30]. Consistent with previous studies[4,31], we found DOX contributed to cardiac ferroptosis manifested by lipid peroxidation, iron overload, and mitochondrial damage, and idebenone could significantly attenuate this novel regulated cell death after DOX treatment *in vitro* and *in vivo*. Ferroptosis usually occurs in response to disruptions in intracellular iron levels. Our data showed that idebenone improved DOX-induced disturbance of iron metabolism. Specifically, iron input increases after DOX treatment, Fe^{3+} in intracellular ferritin is converted to Fe^{2+}, unstable iron pools accumulate, and the Fenton reaction causes intracellular ROS species to increase[3,32], which were reversed by idebenone through regulating TFR1 and FTH1. Additionally, idebenone treatment also attenuated DOX-induced cardiomyocyte apoptosis, which is a classical pathological phenotype of DOX-induced cardiotoxicity[15].

Ferroptosis molecular mechanisms are complex and affected by multiple cellular processes. However, the main intracellular ferroptotic antioxidant systems are GPX4 and FSP1. In this study, we confirmed that idebenone regulates DOX-induced ferroptosis in interaction with the FSP1 protein, as shown by CESTA, BLI, and molecular docking results. FSP1, originally called AIFM2, is a NADPH-dependent oxidoreductase, that reduces CoQ_{10} to $CoQ_{10}H_2$[10,20]. Similar to the GPX4−GSH redox axis, FSP1−CoQ_{10} is an independent defense system against ferroptosis. Interestingly, GPX4 is a crucial gene for mouse growth and development[33,34], while FSP1 is not required[21]. Thus, targeting FSP1 is safer and may have relatively fewer adverse effects on cardiac physiology and development. Currently, there are no drugs in clinical trials targeting the FSP1−CoQ_{10} pathway. In this study, we found that idebenone upregulated the protein level of FSP1 in DOX-treated hearts and NRCMs. Further experiments showed that idebenone treatment increased the $CoQ_{10}H_2/CoQ_{10}$ ratio. FSP1 inhibition abolished the positive effect of idebenone on DOX-induced ferroptosis, and enhanced sensitivity to DOX-induced ferroptosis. In view of FSP1's ability to reduce CoQ_{10}, we used 4-CBA to inhibit the synthesis of CoQ_{10}. And the results showed that 4-CBA significantly inhibited the effect of idebenone on DOX-induced ferroptosis. As we know, protein levels are mainly regulated by the mRNA transcription or protein degradation pathway. Previous studies have shown that the mRNA level of *Fsp1* is regulated by the kEAP1−NRF2 axis[21]. Alternatively, recent reports have shown that ACSL1 regulates the myristoylation of FSP1 and enhances FSP1 membrane recruitment[22]. Interestingly, idebenone did not alter the transcript levels of FSP1 and idebenone is not involved in FSP1 proteostasis through the autophagy pathway. Therefore, idebenone may regulate FSP1 protein level through the ubiquitin−proteasome pathway. Treatment with protein biosynthesis inhibitor cycloheximide or proteasome inhibitor MG-132 confirmed that idebenone does not affect FSP1 protein production, but may affect its proteasome degradation pathway. Molecular docking showed that idebenone formed a stable hydrogen bond interaction with FSP1, especially at Lys118 and Lys355, which may affect the ubiquitination-bound lysine sites of FSP1. Further, co-immunoprecipitation confirmed that idebenone treatment could significantly downregulate the ubiquitination level of FSP1, thereby inhibiting FSP1 degradation. Plasmid transfection and Co-IP results further indicated that idebenone may regulate FSP1 protein homeostasis by interacting with the K355 site of FSP1.

Although our study provides strong evidence for idebenone's therapeutic effect on DOX-induced cardiotoxicity, it has several limitations. First, the effect of idebenone on female mice was not evaluated. Previous studies reported that DOX-induced cardiotoxicity was more pronounced in male patients[35], but it will be essential to determine the effect of sex hormone levels on idebenone effects in follow-up experiments. On the other hand, the effects of idebenone metabolites on DOX-induced cardiotoxicity and ferroptosis were not evaluated. Finally, the role of idebenone in chemotherapy patients remains largely unknown, and its translation to clinical therapy still requires more research.

5. Conclusions

In summary, we discovered that idebenone protects against DOX-induced cardiotoxicity by inhibiting ferroptosis, in part through the regulation of FSP1. Our investigation further revealed that idebenone obstructs the ubiquitination of FSP1, thus impeding its proteolytic degradation, through stable binding to the K355 site of FSP1. Given these novel findings, idebenone may hold potential for use as a clinical therapeutic agent for treating DOX-induced cardiotoxicity.

Acknowledgments

The work was supported by the following grants: the Regional Innovation and Development Joint Fund of the National Natural Science Foundation of China (No. U22A20269); the National Key R&D Program of China (No. 2018YFC1311300); the National Natural Science Foundation of China (Nos. 82200262 and 82000229).

Author contributions

Qizhu Tang, Hongliang Qiu, Sihui Huang, Yuting Liu and Man Xu conceived and designed this study. Hongliang Qiu, Yuting Liu, Libo Liu, Fengming Guo, Yingying Guo, Dan Li and Xianfeng Cen performed the experiments and collected the data. Hongliang Qiu, Yuting Liu, Yajie Chen, Meng Zhang and Yan Che prepared graphs and analyzed the data. Hongliang Qiu wrote the manuscript. Qizhu Tang, Man Xu and Sihui Huang revised the manuscript. All authors discussed and approved the manuscript.

Conflicts of interest

All authors declare that there are no conflicts of interest.

Appendix A. Supporting information

Supporting data to this article can be found online at https://doi.org/10.1016/j.apsb.2024.03.015.

References

1. Swain SM, Whaley FS, Ewer MS. Congestive heart failure in patients treated with doxorubicin: a retrospective analysis of three trials. *Cancer* 2003;**97**:2869–79.
2. Pan JA, Zhang H, Lin H, Gao L, Zhang HL, Zhang JF, et al. Irisin ameliorates doxorubicin-induced cardiac perivascular fibrosis through inhibiting endothelial-to-mesenchymal transition by regulating ROS accumulation and autophagy disorder in endothelial cells. *Redox Biol* 2021;**46**:102120.
3. Pan J, Xiong W, Zhang A, Zhang H, Lin H, Gao L, et al. The imbalance of p53–Park7 signaling axis induces iron homeostasis dysfunction in doxorubicin-challenged cardiomyocytes. *Adv Sci (Weinh)* 2023;**10**:e2206007.
4. Fang X, Wang H, Han D, Xie E, Yang X, Wei J, et al. Ferroptosis as a target for protection against cardiomyopathy. *Proc Natl Acad Sci U S A* 2019;**116**:2672–80.
5. Li N, Jiang W, Wang W, Xiong R, Wu X, Geng Q. Ferroptosis and its emerging roles in cardiovascular diseases. *Pharmacol Res* 2021;**166**:105466.
6. Yu W, Hu Y, Liu Z, Guo K, Ma D, Peng M, et al. Sorting nexin 3 exacerbates doxorubicin-induced cardiomyopathy *via* regulation of TFRC-dependent ferroptosis. *Acta Pharm Sin B* 2023;**13**:4875–92.
7. Dixon SJ, Lemberg KM, Lamprecht MR, Skouta R, Zaitsev EM, Gleason CE, et al. Ferroptosis: an iron-dependent form of non-apoptotic cell death. *Cell* 2012;**149**:1060–72.
8. Yang WS, SriRamaratnam R, Welsch ME, Shimada K, Skouta R, Viswanathan VS, et al. Regulation of ferroptotic cancer cell death by GPX4. *Cell* 2014;**156**:317–31.
9. Tong J, Li D, Meng H, Sun D, Lan X, Ni M, et al. Targeting a novel inducible GPX4 alternative isoform to alleviate ferroptosis and treat metabolic-associated fatty liver disease. *Acta Pharm Sin B* 2022;**12**:3650–66.
10. Bersuker K, Hendricks JM, Li Z, Magtanong L, Ford B, Tang PH, et al. The CoQ oxidoreductase FSP1 acts parallel to GPX4 to inhibit ferroptosis. *Nature* 2019;**575**:688–92.
11. Mao C, Liu X, Zhang Y, Lei G, Yan Y, Lee H, et al. DHODH-mediated ferroptosis defence is a targetable vulnerability in cancer. *Nature* 2021;**593**:586–90.
12. Buyse GM, Voit T, Schara U, Straathof CSM, D'Angelo MG, Bernert G, et al. Efficacy of idebenone on respiratory function in patients with Duchenne muscular dystrophy not using glucocorticoids (DELOS): a double-blind randomised placebo-controlled phase 3 trial. *Lancet* 2015;**385**:1748–57.
13. Gueven N, Ravishankar P, Eri R, Rybalka E. Idebenone: when an antioxidant is not an antioxidant. *Redox Biol* 2021;**38**:101812.
14. Jiang W, Geng H, Lv X, Ma J, Liu F, Lin P, et al. Idebenone protects against atherosclerosis in apolipoprotein E-deficient mice *via* activation of the SIRT3–SOD2–mtROS pathway. *Cardiovasc Drugs Ther* 2021;**35**:1129–45.
15. Zhang X, Hu C, Kong CY, Song P, Wu HM, Xu SC, et al. FNDC5 alleviates oxidative stress and cardiomyocyte apoptosis in doxorubicin-induced cardiotoxicity *via* activating AKT. *Cell Death Differ* 2020;**27**:540–55.
16. Liu LB, Huang SH, Qiu HL, Cen XF, Guo YY, Li D, et al. Limonin stabilises sirtuin 6 (SIRT6) by activating ubiquitin specific peptidase 10 (USP10) in cardiac hypertrophy. *Br J Pharmacol* 2022;**179**:4516–33.
17. Xie S, Xing Y, Shi W, Zhang M, Chen M, Fang W, et al. Cardiac fibroblast heat shock protein 47 aggravates cardiac fibrosis post myocardial ischemia–reperfusion injury by encouraging ubiquitin specific peptidase 10 dependent Smad4 deubiquitination. *Acta Pharm Sin B* 2022;**12**:4138–53.
18. Trott O, Olson AJ. AutoDock Vina: improving the speed and accuracy of docking with a new scoring function, efficient optimization, and multithreading. *J Comput Chem* 2010;**31**:455–61.
19. Fang X, Ardehali H, Min J, Wang F. The molecular and metabolic landscape of iron and ferroptosis in cardiovascular disease. *Nat Rev Cardiol* 2023;**20**:7–23.
20. Doll S, Freitas FP, Shah R, Aldrovandi M, da Silva MC, Ingold I, et al. FSP1 is a glutathione-independent ferroptosis suppressor. *Nature* 2019;**575**:693–8.
21. Koppula P, Lei G, Zhang Y, Yan Y, Mao C, Kondiparthi L, et al. A targetable CoQ-FSP1 axis drives ferroptosis- and radiation-resistance in KEAP1 inactive lung cancers. *Nat Commun* 2022;**13**:2206.
22. Zhang Q, Li N, Deng L, Jiang X, Zhang Y, Lee LTO, et al. ACSL1-induced ferroptosis and platinum resistance in ovarian cancer by increasing FSP1 *N*-myristylation and stability. *Cell Death Discov* 2023;**9**:83.
23. Yuan J, Lv T, Yang J, Wu Z, Yan L, Yang J, et al. HDLBP-stabilized lncFAL inhibits ferroptosis vulnerability by diminishing Trim69-dependent FSP1 degradation in hepatocellular carcinoma. *Redox Biol* 2022;**58**:102546.
24. Kalyanaraman B. Teaching the basics of the mechanism of doxorubicin-induced cardiotoxicity: have we been barking up the wrong tree? *Redox Biol* 2020;**29**:101394.
25. Liu YT, Che Y, Qiu HL, Xia HX, Feng YZ, Deng JY, et al. ADP-ribosylation: an emerging direction for disease treatment. *Ageing Res Rev* 2023;**94**:102176.
26. Tebbi CK, London WB, Friedman D, Villaluna D, De Alarcon PA, Constine LS, et al. Dexrazoxane-associated risk for acute myeloid leukemia/myelodysplastic syndrome and other secondary malignancies in pediatric Hodgkin's disease. *J Clin Oncol* 2007;**25**:493–500.
27. Borrelli E, Berni A, Cascavilla ML, Barresi C, Battista M, Lari G, et al. Visual outcomes and optical coherence tomography biomarkers of vision improvement in patients with leber hereditary optic neuropathy treated with idebenone. *Am J Ophthalmol* 2023;**247**:35–41.

28. Huang Y, Ma M, Zhu X, Li M, Guo M, Liu P, et al. Effectiveness of idebenone nanorod formulations in the treatment of Alzheimer's disease. *J Control Release* 2021;**336**:169−80.
29. Li D, Zhang G, Wang Z, Guo J, Liu Y, Lu Y, et al. Idebenone attenuates ferroptosis by inhibiting excessive autophagy *via* the ROS−AMPK−mTOR pathway to preserve cardiac function after myocardial infarction. *Eur J Pharmacol* 2023;**943**:175569.
30. Zhu X, Wang X, Zhu B, Ding S, Shi H, Yang X. Disruption of histamine/H_1R−STAT3−SLC7A11 axis exacerbates doxorubicin-induced cardiac ferroptosis. *Free Radic Biol Med* 2022;**192**:98−114.
31. Wang Y, Yan S, Liu X, Deng F, Wang P, Yang L, et al. PRMT4 promotes ferroptosis to aggravate doxorubicin-induced cardiomyopathy *via* inhibition of the Nrf2/GPX4 pathway. *Cell Death Differ* 2022;**29**:1982−95.
32. Miranda CJ, Makui H, Soares RJ, Bilodeau M, Mui J, Vali H, et al. Hfe deficiency increases susceptibility to cardiotoxicity and exacerbates changes in iron metabolism induced by doxorubicin. *Blood* 2003;**102**:2574−80.
33. Hangauer MJ, Viswanathan VS, Ryan MJ, Bole D, Eaton JK, Matov A, et al. Drug-tolerant persister cancer cells are vulnerable to GPX4 inhibition. *Nature* 2017;**551**:247−50.
34. Yant LJ, Ran Q, Rao L, Van Remmen H, Shibatani T, Belter JG, et al. The selenoprotein GPX4 is essential for mouse development and protects from radiation and oxidative damage insults. *Free Radic Biol Med* 2003;**34**:496−502.
35. Cadeddu Dessalvi C, Pepe A, Penna C, Gimelli A, Madonna R, Mele D, et al. Sex differences in anthracycline-induced cardiotoxicity: the benefits of estrogens. *Heart Fail Rev* 2019;**24**:915−25.